Information Sciences 322 (2015) 20–30

Contents lists available at ScienceDirect

Information Sciences

journal homepage: www.elsevier.com/locate/ins

QTC_{3D}: Extending the qualitative trajectory calculus to three dimensions

Nikolaos Mavridis [a], Nicola Bellotto [b,*], Konstantinos Iliopoulos [a], Nico Van de Weghe [c]

[a] Institute of Informatics and Telecommunication, NCSR Demokritos, Greece
[b] School of Computer Science, University of Lincoln, United Kingdom
[c] Department of Geography, Ghent University, Belgium

ARTICLE INFO

Article history:
Received 12 February 2014
Received in revised form 5 March 2015
Accepted 5 June 2015
Available online 16 June 2015

Keywords:
Qualitative representations
Qualitative Trajectory Calculus (QTC)
Moving objects
Spatio-temporal modeling

ABSTRACT

Spatial interactions between agents (humans, animals, or machines) carry information of high value to human or electronic observers. However, not all the information contained in a pair of continuous trajectories is important and thus the need for qualitative descriptions of interaction trajectories arises. The Qualitative Trajectory Calculus (QTC) (Van de Weghe, 2004) is a promising development towards this goal. Numerous variants of QTC have been proposed in the past and QTC has been applied towards analyzing various interaction domains. However, an inherent limitation of those QTC variations that deal with lateral movements is that they are limited to two-dimensional motion; therefore, complex three-dimensional interactions, such as those occurring between flying planes or birds, cannot be captured. Towards that purpose, in this paper QTC_{3D} is presented: a novel qualitative trajectory calculus that can deal with full three-dimensional interactions. QTC_{3D} is based on transformations of the Frenet–Serret frames accompanying the trajectories of the moving objects. Apart from the theoretical exposition, including definition and properties, as well as computational aspects, we also present an application of QTC_{3D} towards modeling bird flight. Thus, the power of QTC is now extended to the full dimensionality of physical space, enabling succinct yet rich representations of spatial interactions between agents.

1. Introduction

As the epitome of the philosophy of Heraclitus (544-484BC) states: "*All entities move and nothing remains still*". Thus *change*, and especially *motion* (which is the primary sensory manifestation of change), are central elements in almost all philosophical–conceptual systems. The simplest conception of motion is absolute motion, which describes the movement of an entity with respect to a stationary frame of reference. However, moving beyond the absolute motion of an individual entity, one of the most important species of motion is relative motion between two entities, which forms an essential aspect of special interaction, for the case of objects construed as agents (humans, animals, or machines). Such spatial interactions between agents carry information of high value to *human observers*, as exemplified by the high-level interpretations and judgments that humans make when watching the Heider and Simmel movie [14],[1] or by the rich semantic content of moving point abstractions of

* Corresponding author.
E-mail address: nbellotto@lincoln.ac.uk (N. Bellotto).

[1] In this classic psychological experiment, a movie is shown to experimental subjects, where a set of simple geometrical figures (triangles, points, and lines) move in trajectories with respect to one another. However, when humans are asked to report what they have seen, they directly offer anthropocentric (or arguably, biocentric) interpretations of what they have seen: the triangles are reported as having affective state (angry, afraid, etc.), their relative motions are interpreted as intentional acts (chasing, confronting, hiding) and so on. All of this rich information is included not in the form of the figures, but just in the relative trajectories of them.

http://dx.doi.org/10.1016/j.ins.2015.06.002
0020-0255/

real-world events and everyday interaction scenes (e.g. reading gender from gait, [21]). Furthermore, such spatial interactions between agents carry invaluable information not only to human observers, but increasingly also to *electronic sensing systems*, for example those overlooking or assisting with crowd flows [32], or traffic management [5]. In recent years, geographical information scientists have intensively explored the relationships between multiple moving point objects. Research in this area has predominantly focused on the comparison of quantitative characteristics of trajectories such as azimuth, velocity, turning angle, acceleration, and sinuosity. An extensive overview is given in Long and Nelson [19].

However, when observing the relative motion between two agents, not all the information contained in a pair of continuous trajectories is always important. For example, one might not really need the exact distance between two agents, but only the trend of change of relative distance or pose between them. Thus, the need for qualitative descriptions of interaction trajectories arises, abstracting unnecessarily complex complete quantitative representations. An adaptive representation of spatial trajectories of pairs or groups of objects, which can retain exactly as much qualitative information as needed for each application, can also be used for learning and reproducing interactive behaviors.

The Qualitative Trajectory Calculus (QTC), devised by Van de Weghe [26], is a promising development towards this goal. A number of variants of QTC have been proposed in the past, including versions enabling the application of QTC to networks [8], and shapes [31]. However, an inherent limitation of the existing variations of QTC considering lateral movements (e.g. QTC Double Cross) is that they can only deal with two-dimensional motion. Therefore, complex three-dimensional interactions, such as those occurring between flying planes or birds, cannot be adequately captured. Towards such purpose, in this paper we propose QTC_{3D}: the first extension of QTC that can specifically deal with three-dimensional interactions.

Our representation is based on qualitative descriptions of transformations of the Frenet–Serret frames [17] accompanying the trajectories of the moving objects. In more detail, the two Frenet–Serret frames corresponding to the two moving points consist of the tangent, normal, and binormal vectors. The relative motion between the two frames is modeled by the transformation that maps one frame to the other. Apart from the continuous model, the proper application of QTC_{3D} in real-world sampled trajectories also requires proper discretization, which is also devised and presented. Finally, an example application towards qualitative modeling of the flight of a flock of birds is provided, illustrating the elegance and power of QTC_{3D} for a compact representation of complex three-dimensional interactions while ignoring unnecessary detail and exposing only essential information.

In this paper, we will proceed in Section 2 by providing a discussion of relevant existing literature, followed in Section 3 by a theoretical explanation including the definition of QTC_{3D} and its fundamental properties. Then, in Section 4, we will discuss computational aspects, and provide a version of QTC_{3D} that can deal with discrete-time sampled trajectories. In Section 5, we present an illustrative example of QTC_{3D} towards modeling bird flight. Finally, we will close with a discussion, including future steps, followed by a conclusion. Overall, and most importantly, through this paper, the power of QTC will be extended to the full dimensionality of physical space, enabling succinct yet rich representations of spatial interactions between agents.

2. Background

Qualitative temporal and spatial reasoning about movement behavior has increasingly gained momentum over the last two decades, as scholars have begun to recognize the importance of qualitative reasoning in describing the common-sense background knowledge on which our human perspective on physical movements is based [11,12]. In particular, various qualitative temporal calculi, such as the *Interval Calculus* [2] and the *Semi Interval Calculus* [10], have been proposed. Along this line, a well-matured body of research has been developed regarding mereotopological relationships, as exemplified by the *RCC-calculus* [25] and the *9-intersection model* [9].

Until recently however, there was a lack of academic work on calculi to represent trajectories of disjoint objects, hampering applications where most objects are disconnected, such as moving vehicles, pedestrians and animals. To address this shortcoming, Van de Weghe [26] introduced the *Qualitative Trajectory Calculus* (QTC) to describe the relative motion of disconnected moving objects, providing an answer for many trajectory applications. As with other qualitative calculi, the theoretical framework of QTC has been thoroughly investigated by, among others, composition-tables [28] and conceptual neighborhood diagrams [29]. This has been furthered by an implementation of QTC that is capable of describing real-world movements, both at time stamps (by $QTC_{relations}$) and during longer periods (by $QTC_{animations}$, being a sequence of $QTC_{relations}$) [7]. Such animations can represent all kinds of real-world interactions, including an overtake event [27] and prey–predator interactions [30].

Recently, QTC has been applied to analyze and implement human–robot spatial interactions. In the preliminary work of Bellotto [3], a version of QTC dealing only with the linear distance between two agents (i.e. QTC Basic = QTC_B) was adopted to describe and implement simple spatial interactions, in which a robot and a human approached or moved away from each other. In Hanheide et al. [13], the human trajectory induced by a particular robot motion behavior in narrow spaces was analyzed using sequences of QTC states that included also lateral movements (i.e. QTC Double Cross = QTC_C). Combinations of QTC_B and QTC_C sequences were then exploited in Bellotto et al. [4] to design and implement human–robot spatial interactions with varying degrees of resolution, depending on the scenario and the desired robot's behavior. In all these cases, however, only 2D trajectories have been considered. The reason behind this is simple: in two dimensions, a unique line interconnecting the two moving points can be drawn, which divides the plane in two clearly defined regions. In three dimensions, a unique plane cannot be constructed between two points, and therefore no such clear partition exists.

Some previous work has considered qualitative spatial representations and reasoning on 3D regions [1]. Also, an attempt has been made on the orientation of point objects, but only with respect to external reference systems [23,24]. Furthermore, the complexity of the proposed models could limit their implementation and actual application to real-world problems. Thus, we need to resort to a novel constraint for QTC, in order to be able to capture the richness of interactions of a pair of three dimensional moving point objects.

3. Definition and properties

3.1. A brief overview of QTC_{2D}

Let us start by providing a brief summary of the essentials of the traditional two-dimensional Qualitative Trajectory Calculus [26]. The properties that QTC_{2D} can retain are all the following ones, or specific subsets of them:

- Q_1: Distance constraint for the first object, conventionally named *k*:
  − means that it is approaching the second object, named *l*,
  + means that it is moving further away, and
  0 means that its distance remains steady.
- Q_2: Distance constraint, similar to Q_1 but with the objects *k* and *l* interchanged.
- Q_3: Speed constraint; because of the dual nature we only need one such constraint:
  − means that object *k* is slower than *l*,
  + means that *k* is faster than *l*, and
  0 means that they move with the same speed.
- Q_4: Side constraint for *k* with respect to vector *kl*:
  − means that *k* is moving to the left of the line,
  + means that *k* is moving to the right of the line, and
  0 means that it moves along the line.
- Q_5: Side constraint, similar to Q_4 but with the roles of *k* and *l* interchanged.
- Q_6: Angle constraint: define as θ_k the minimum absolute angle (MAA) between the velocity vector v_k of *k* and vector *kl*, and θ_l the equivalent for the velocity v_l of *l*. Then we obtain
  − if $\theta_k < \theta_l$, i.e. *k* is moving at a smaller angle with respect to *kl* than *l*,
  +if $\theta_k > \theta_l$, i.e. the inverse of the above,
  0 for all other cases, i.e. *k* and *l* are moving at the same angle with respect to *kl*.

Note that the constraint Q_6 does not hold any particular information regarding the alignment of the two agents. Such qualitative insight can only be extracted by observing other constraints or combinations of them.

In order to help the readers better understand the above concepts, we provide the trajectories of two Moving Point Objects (MPOs) in Fig. 1 and the corresponding values of the constraints in Table 1.

By deciding to retain different subsets of the above constraints, we can obtain the following calculi, listed here in order of increasing complexity:

- QTC_{B1}: Supports relations Q_1 and Q_2.
- QTC_{B2}: Supports relations Q_1 through Q_3.
- QTC_{C1}: Supports relations Q_1, Q_2, Q_4, and Q_5.
- QTC_{C2}: Supports relations Q_1 through Q_6.

For further explanation with respect to typical aspects of qualitative reasoning (e.g. dominance space, conceptual neighborhood diagrams, composition tables), we refer to Van de Weghe [26].

3.2. Introducing QTC_{3D}

When extending QTC from 2D to 3D, analogous constraints to those outlined above have to be devised. Distance constraints (Q_1, Q_2), Speed constraint (Q_3), and Angle constraint (Q_6) can be easily generalized. However, as previously mentioned, there is no obvious analogue to the Side constraints (Q_4, Q_5).

The Frenet–Serret frame was thus chosen as our main instrument, as it provides a rich description of the kinetic properties of an object moving along a continuous and differentiable trajectory. The frame consists of three orthogonal vectors (see also Fig. 2 and Eqs. (I)–(III)):

t: the unit vector tangent to the curve;
n: the normal unit vector;
b: the binormal unit vector, i.e. a vector perpendicular to both ***t*** and ***n***.

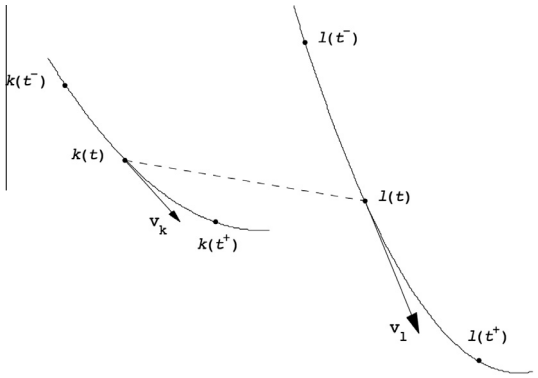

Fig. 1. Trajectories of two MPOs.

Table 1
Constraints and their values for the MPOs of Fig. 1.

Constraint	Value	Explanation
Q_1	–	k is moving towards l
Q_2	+	l is moving away from k
Q_3	–	k is slower than l
Q_4	+	k is moving towards the right side of vector kl
Q_5	–	l is moving towards the left side of vector lk
Q_6	–	the angle between v_k and vector kl is smaller than the angle between v_l and vector lk

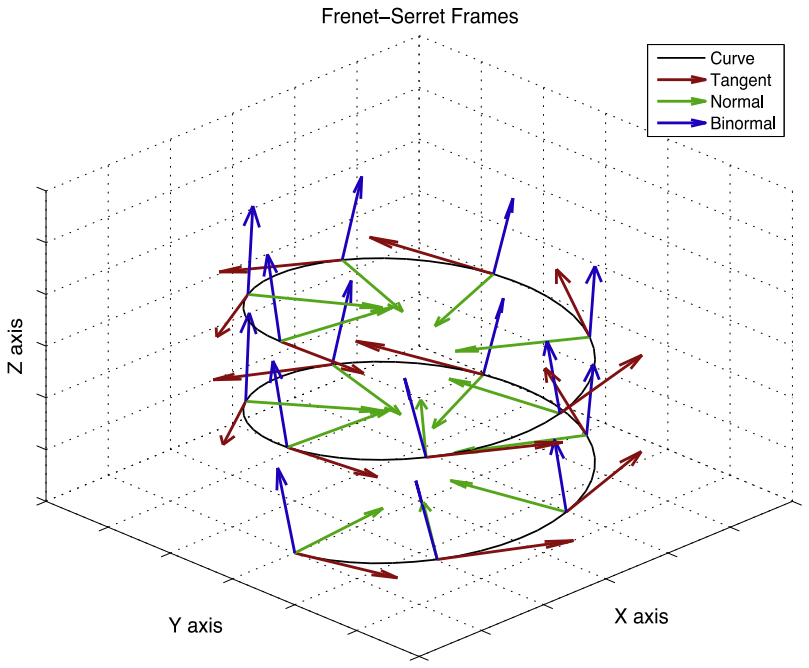

Fig. 2. Illustration of the Frenet–Serret frame.

The three vectors $\boldsymbol{t}, \boldsymbol{n}$, and $\boldsymbol{b}$, create an orthonormal frame of reference for each point in the trajectory (Fig. 2). Most importantly, this is a non-inertial frame, and one can furthermore prove that it is particularly well behaved with regards to Euclidean motions, i.e. rotations and translations.

Given two continuous three-dimensional trajectories $\boldsymbol{s_1}(\tau)$ and $\boldsymbol{s_2}(\tau)$, where τ is the continuous time variable, $\boldsymbol{s}$ is the position parameter, and $\boldsymbol{s}(\tau)$ is twice continuously differentiable,[2] the new QTC_{3D} is constructed as follows:

[2] If one wants smoothness, then C1 continuity is enough; but if one needs smoothness *and* continuous curvatures, then one needs C2 continuity. This is not an extra requirement for specifically, but holds anywhere continuity of curvature is needed.

STEP(1) Calculate signs $(-,0,+)$ for all constraints Q_1, Q_2, Q_3, and Q_6 as defined for QTC_{2D} generalized from 2D to 3D;
STEP(2) Calculate the component vectors of the two Frenet–Serret frames, i.e. the tangents, normals, and binormals, according to the following equations [20]:

$$\boldsymbol{t}_1(\tau) = (d\boldsymbol{s}_1/d\tau)/|d\boldsymbol{s}_1/d\tau| \quad \boldsymbol{t}_2(\tau) = (d\boldsymbol{s}_2/d\tau)/|d\boldsymbol{s}_2/d\tau| \tag{I}$$
$$\boldsymbol{n}_1(\tau) = (d\boldsymbol{t}_1/d\tau)/|d\boldsymbol{t}_1/d\tau| \quad \boldsymbol{n}_2(\tau) = (d\boldsymbol{t}_2/d\tau)/|d\boldsymbol{t}_2/d\tau| \tag{II}$$
$$\boldsymbol{b}_1(\tau) = \boldsymbol{t}_1(\tau) \times \boldsymbol{n}_1(\tau) \quad \boldsymbol{b}_2(\tau) = \boldsymbol{t}_2(\tau) \times \boldsymbol{n}_2(\tau) \tag{III}$$

Now, our aim is to transform the frame $\boldsymbol{F_1}(\boldsymbol{t_1}, \boldsymbol{n_1}, \boldsymbol{b_1})$ of the first moving object, to the frame $\boldsymbol{F_2}(\boldsymbol{t_2}, \boldsymbol{n_2}, \boldsymbol{b_2})$ of the second moving object at the same time stamp. We thus need to find a transformation $\boldsymbol{T}$ transforming the first frame to the second:

$$\boldsymbol{F_2} = \boldsymbol{T}\boldsymbol{F_1} \Rightarrow \boldsymbol{T} = \boldsymbol{F_2}\boldsymbol{F_1^{-1}} \tag{IV}$$

This transformation $\boldsymbol{T}$ can be decomposed as the product of three rotations, which are usually known in the aeronautics literature as the yaw ψ, pitch θ, and roll φ (i.e. the so-called Tait-Bryan angles), as illustrated in Fig. 3.

We thus need to compute the three angles corresponding to the component rotations that multiply out to $\boldsymbol{T}$, as defined below:

$$\boldsymbol{T} = \begin{bmatrix} r_{11} & r_{12} & r_{13} \\ r_{21} & r_{22} & r_{23} \\ r_{31} & r_{32} & r_{33} \end{bmatrix}$$
$$\psi = atan2(r_{21}, r_{11}), \quad \psi \in (-\pi, \pi] \tag{V}$$
$$\theta = atan2\left(-r_{31}, \sqrt{r_{32}^2 + r_{33}^2}\right), \quad \theta \in (-\pi, \pi]$$
$$\varphi = atan2(r_{32}, r_{33}), \quad \varphi \in (-\pi, \pi]$$

It is easy to perform the inverse process and justify that the yaw, pitch, and roll rotations lead to a valid composite rotation matrix. Consider the following rotations:

$$\boldsymbol{R}(\psi) = \begin{pmatrix} \cos\psi & -\sin\psi & 0 \\ \sin\psi & \cos\psi & 0 \\ 0 & 0 & 1 \end{pmatrix}$$
$$\boldsymbol{R}(\theta) = \begin{pmatrix} \cos\theta & 0 & \sin\theta \\ 0 & 1 & 0 \\ -\sin\theta & 0 & \cos\theta \end{pmatrix} \tag{VI}$$
$$\boldsymbol{R}(\varphi) = \begin{pmatrix} 1 & 0 & 0 \\ 0 & \cos\varphi & -\sin\varphi \\ 0 & \sin\varphi & \cos\varphi \end{pmatrix}$$

Performing the roll, pitch, and yaw rotations (in that order), would yield the following matrix [18], which corresponds to our transformation $\boldsymbol{T}$:

$$\boldsymbol{R}(\psi, \theta, \varphi) = \begin{pmatrix} \cos\psi\cos\theta & \cos\psi\sin\theta\sin\varphi - \sin\psi\cos\varphi & \cos\psi\sin\theta\cos\varphi + \sin\psi\sin\varphi \\ \sin\psi\cos\theta & \sin\psi\sin\theta\sin\varphi + \cos\psi\cos\varphi & \sin\psi\sin\theta\cos\varphi - \cos\psi\sin\varphi \\ -\sin\theta & \cos\theta\sin\varphi & \cos\theta\cos\varphi \end{pmatrix} \tag{VII}$$

Moving on, and in order to derive a meaningful qualitative representation for the quantitative representation of the three angles (ψ, θ, φ), we need to quantize all possible values of this triplet to a set of qualitative symbols, $(-,0,+)$ in QTC. For the ideal case of continuous trajectories (i.e. sampled with infinite uncountable sampling rate, and without corruption by measurement noise), we define the QTC symbols for each angle $\alpha \in \{\psi, \theta, \varphi\}$:

- if $\alpha < 0 \rightarrow$ '–',
- if $\alpha = 0 \rightarrow$ '0',
- if $\alpha > 0 \rightarrow$ '+'.

Thus, through this procedure, we derive the new QTC symbols Q_7, Q_8, Q_9 for the angles ψ, θ, φ, respectively, which, in conjunction with the above Q_1, Q_2, Q_3, and Q_6, comprise the full QTC_{3D} representation Q_1, Q_2, Q_3, Q_6, Q_7, Q_8, Q_9.

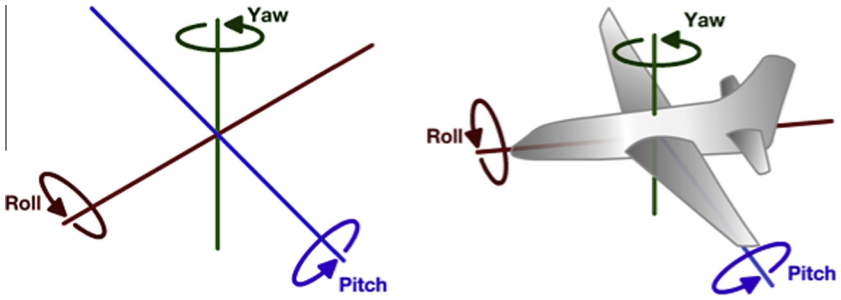

Fig. 3. Yaw, pitch, and roll angles.

4. From ideal-continuous time to real-discrete time

In order to apply the above in real-world time-sampled trajectories, one can use the Discrete Frenet–Serret Frame [15,20]. If no three consecutive points of the discrete curve are collinear (i.e. $\boldsymbol{t_1}$ and $\boldsymbol{t_2}$ are not parallel), Eqs. (I)–(III) become the following:

$$\begin{aligned}\boldsymbol{t_1}(\tau) &= (\boldsymbol{x_1}(\tau+1) - \boldsymbol{x_1}(\tau))/|\boldsymbol{x_1}(\tau+1) - \boldsymbol{x_1}(\tau)| \\ \boldsymbol{t_2}(\tau) &= (\boldsymbol{x_2}(\tau+1) - \boldsymbol{x_2}(\tau))/|\boldsymbol{x_2}(\tau+1) - \boldsymbol{x_2}(\tau)|\end{aligned} \tag{VIII}$$

$$\begin{aligned}\boldsymbol{b_1}(\tau) &= (\boldsymbol{t_1}(\tau-1) \times \boldsymbol{t_1}(\tau))/|\boldsymbol{t_1}(\tau-1) \times \boldsymbol{t_1}(\tau)| \\ \boldsymbol{b_2}(\tau) &= (\boldsymbol{t_2}(\tau-1) \times \boldsymbol{t_2}(\tau))/|\boldsymbol{t_2}(\tau-1) \times \boldsymbol{t_2}(\tau)|\end{aligned} \tag{IX}$$

$$\begin{aligned}\boldsymbol{n_1}(\tau) &= \boldsymbol{b_1}(\tau) \times \boldsymbol{t_1}(\tau) \\ \boldsymbol{n_2}(\tau) &= \boldsymbol{b_2}(\tau) \times \boldsymbol{t_2}(\tau)\end{aligned} \tag{X}$$

The discrete frames are:

$$\boldsymbol{F_1}(\tau) = (\boldsymbol{t_1}(\tau), \boldsymbol{n_1}(\tau), \boldsymbol{b_1}(\tau)), \quad \boldsymbol{F_2}(\tau) = (\boldsymbol{t_2}(\tau), \boldsymbol{n_2}(\tau), \boldsymbol{b_2}(\tau))$$

The yaw, pitch, and roll angles are then calculated similarly to the continuous case. As can be seen in the equation below, for the quantization of continuous angle values to the three discrete symbols $(-, 0, +)$, a threshold Th is used in this real-world case.[3] This is required in order to delineate a symmetric band around the zero value of the angles, so that numerical deviations as well as measurement noise can be accounted for.

Thus, for $\alpha \in \{\psi, \theta, \varphi\}$ the mapping of values to symbols for the discrete case becomes:

- if $\alpha < -Th \rightarrow$ '−',
- if $-Th \leqslant \alpha \leqslant Th \rightarrow$ '0',
- if $\alpha > Th \rightarrow$ '+'.

In this way, we are able to derive meaningful QTC_{3D} symbol sequences from real-world sampled trajectories.

5. A real-world example

In order to illustrate the utility of QTC_{3D}, we have chosen to apply it in a domain where rich 3D trajectories with complex interactions exist: bird flock flying. We utilize a micro-GPS derived dataset of pigeon flights from a recent paper published in Nature [22]. This dataset contains 4 homing- and 11 free-flights of at least 10 individuals each. We consider in particular the 4 homing flights, where there exists a clear hierarchy of the roles of the pigeons. We then ask the following question: can information about pairs of interacting trajectories encoded in QTC_{3D} be used towards distinguishing leader–follower bird pairs from other pairs? This is a typical interaction studied in reasoning about moving objects. In order to answer such a question, we have performed the following procedure.

First, we selected appropriate trajectory pairs (all of which were sampled at a temporal resolution of 200 ms[4]), with and without Leader–Follower (LF) relations. As an example, let us consider the first of these flights, flight #1. We plot in Fig. 4 the trajectories of all pigeons of homing flight #1. Note that several pigeon trajectories have been truncated, effectively keeping only

[3] The choice of threshold is usually application-specific. The impact of choice, for this specific case, is clearly seen in Fig. 7 and some additional insights are discussed in Section 6. In practice, however, we have found that thresholds $\geqslant 4°$ are adequate.

[4] The 5 Hz (i.e. 200 ms) sampling rate was an inherent limitation of the hardware. However, as justified in the supplementary material to the Nagy et al. [22] paper, this sampling rate was more than adequate for the purpose of analyzing leader/follower relations.

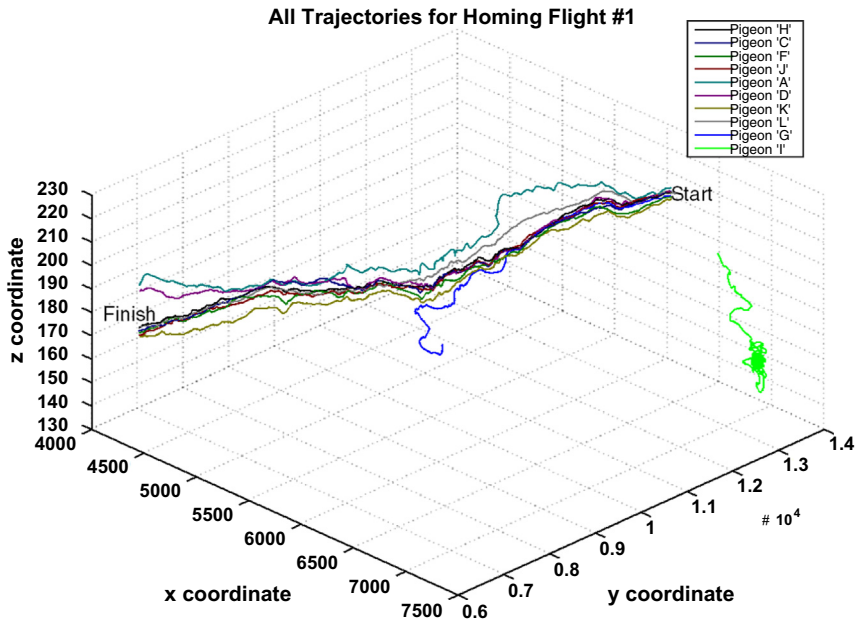

Fig. 4. Truncated flight paths of all the pigeons of homing flight #1.

2000 synchronized data points around the middle of the flight, in order to remove useless data before takeoff and after landing. For the case of LF configurations, we would expect that a change in direction of the leader corresponds to a proportional change in the direction of the follower. That is, if the leader pigeon moves towards a particular direction, then the follower one flights on a parallel direction after a short delay, which depends on the position of the pigeon within the flock hierarchy. In general, to compare these trajectories, one should consider this delay and temporally align the samples. However, in our case there is no need for relative time-shifting of the trajectories, given that the follower response has a delay smaller than the 200 ms sampling interval.

Upon observation of the trajectories for flight #1, we selected pigeon P_H as the Leader. We can then classify the remaining pigeons in two categories, according to whether they closely follow the flight patterns of the leader or they significantly deviate from them:

(a) Followers: pigeons $P_A, P_C, P_D, P_F, P_J, P_K, P_L$.
(b) Non Followers: pigeons P_G, P_I.

Thus, for flight #1, there exist 7 LF trajectory pairs, namely $P_H - P_A, P_H - P_C, P_H - P_D, P_H - P_F, P_H - P_J, P_H - P_K, P_H - P_L$, and 2 Leader–Non-Follower (LNF) trajectory pairs, $P_H - P_G$ and $P_H - P_I$. For flight #2, again we have 1 leader, but this time 6 followers, and 2 non-followers, thus giving 6 LF and 2 LNF pairs. In a similar way, we get 6 LF and 2 LNF for flight #3, and 7 LF and 1 LNF pair for flight #4. Thus, the total number of trajectory pairs, arising from all four flights that we used, is 26 LF and 7 LNF.

We then extract the symbol distributions for all trajectory pairs. When we convert the trajectory pairs to QTC_{3D} strings, they will consist of 7-tuples of $(-, 0, +)$. The important information for our task is contained in the sub-string triplet $\{Q_7, Q_8, Q_9\}$ of the full QTC_{3D} 7-tuple; after all, this is what differentiates QTC_{3D} from QTC_{2D}. In this triplet there exist $3^3 = 27$ possible combinations of symbols. We try to estimate the probability distribution of these combinations by calculating a histogram based on their occurrences. Our ultimate goal in this section will be to differentiate between trajectory pairs of LF and LNF roles: we will show this is possible using the ratio of entropies from the histograms of the QTC_{3D} symbol distributions of LF vs. LNF trajectories, while differentiation would not have been possible using the QTC_{2D} symbols alone (i.e. without the new symbols $\{Q_7, Q_8, Q_9\}$).

First of all, we need to make an informed choice of the appropriate thresholds for the derivation of QTC_{3D}. Towards that purpose, we will first investigate the histograms of the distributions of the Tait-Bryan angles. Figs. 5 and 6 display the histograms of the yaw, pitch, and roll angles, for the LF and LNF respectively, bundled in bins of approximately 8° each. We have chosen this value in order to have enough samples for each bin, so that the resulting curve is smooth and closer to the actual distribution.

In Figs. 5 and 6 (left) we see the frequency distribution of the yaw angles for the aforementioned case of homing flight #1, and we can already identify how discriminative it can be for the possible categories of pairs. If we set the threshold $Th = 24°$, then the total probability mass created by the sum of the central three bins will map to the probability mass of the '0'

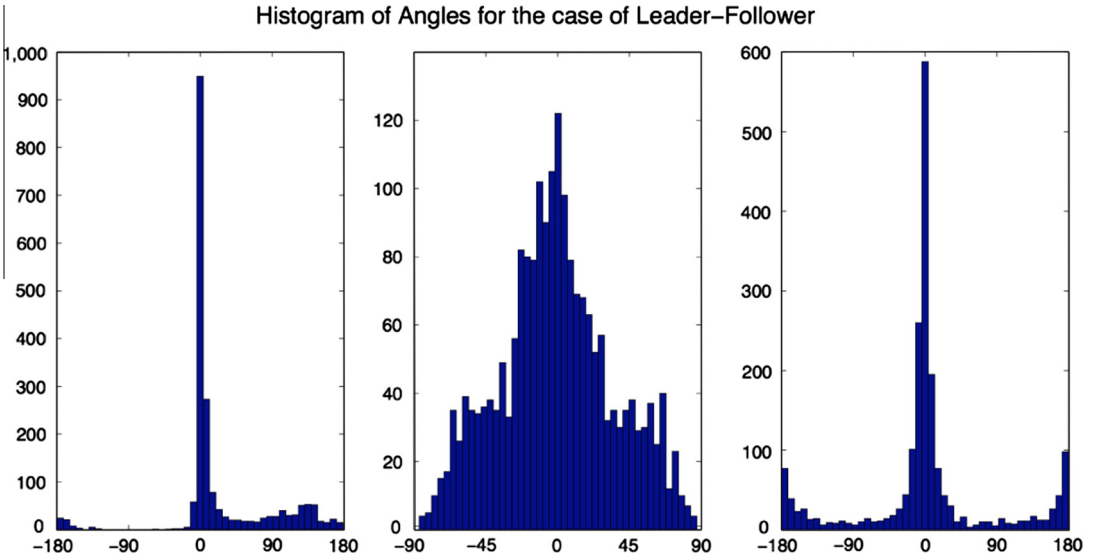

Fig. 5. Yaw, pitch, and roll for the cases of Leader (P_H) and a Follower (P_A).

symbol, while the bins on the right will map to the '+' symbol and the bins on the left will map to '−'. Note that, in the LF case, there will be a larger total mass for the '0' symbol, as the sum of the three central bins for the LF case is larger than the sum of the equivalent ones for the LNF case. Correspondingly, the total mass for each of the '+' or '−' symbols will be smaller for the LF distribution when compared to the LNF one. Thus, if we were taking the entropy of the single symbol corresponding to the yaw angle, the entropy of the LF distribution would be smaller than the entropy of the LNF.

In practice, though, we will use all three angles (yaw, pitch, and roll), not individually but in conjunction in order to create the $3^3 = 27$ possible combinations of symbols, and we will take the entropy over this 27-symbol distribution (and *not* the three entropies of the three 3-symbol distribution corresponding to each angle separately). As we shall see, when we combine the symbols for all three angles, we will expect significantly different probability distributions. The key part is to choose an appropriate threshold *Th* to get a meaningful band of '0' symbols.

Because the LF behavior requires the tracking of the direction of the flight of the leader by the follower, we expect that whenever this direction does not change, the follower will be aligned to it. This will happen not only in terms of direction, but also in terms of velocity and acceleration, if the alignment between leader and follower is to remain and the distance between the two is controlled by the follower with the goal of being kept constant. Thus, the two Frenet–Serret frames will be almost aligned for the period of time that the leader is not changing significantly his trajectory. In this case, the Tait-Bryan angles corresponding to the transformation needed to align one Frenet–Serret frame to the other will frequently have values close to zero. Therefore, the resulting distribution of the quantized QTC symbols corresponding to these angles will exhibit more triplets containing one or more '0's for the LF case, as compared to the LNF one. In the latter case, the two Frenet–Serret frames will be generally more unrelated, and thus the transformation needed to map one to the other will be more random. In conclusion, we expect the distribution of QTC symbols for the yaw, pitch, and roll angles for the LNF case to be closer to uniform (larger entropy) as compared to the symbol distribution for the LF case (smaller entropy, given that the distribution is less uniform).

We then decided to investigate the entropies of the two QTC symbol distributions (i.e. the symbols corresponding to the trajectory of the LF pair, and the symbols corresponding to the LNF pair) and to use these entropies ratio as a discriminative feature for LF vs. LNF pairs. Let $H(X)$ be the entropy of a discrete random variable X and $p(x_i)$ the probability that X takes the QTC_{3D} value x_i:

$$H(X) = -\sum_i p(x_i)\log_2 p(x_i) \tag{XI}$$

In particular, if H_i^{LF} is the entropy of the i-th LF pair, with $i = 1,\ldots,M$, and H_j^{LNF} is the entropy of the j-th LNF pair, with $j = 1,\ldots,N$, the ratio ρ between the two mean entropies μ_{LF} and μ_{LNF} can be calculated as follows:

$$\rho = \frac{\sum_{i=1}^{M} H_i^{LF}}{\sum_{j=1}^{N} H_j^{LNF}} \cdot \frac{N}{M} = \frac{\mu_{LF}}{\mu_{LNF}} \tag{XII}$$

We thus calculated the entropy of the three relevant QTC_{3D} symbols Q_7, Q_8, and Q_9 of all the trajectory pairs of the four flights, i.e. 26 LF and 7 LNF symbol sequences. Indeed, our data indicated that for any appropriate choice of angle threshold $Th \geqslant 5^\circ$, the mean entropy in the LNF case is clearly larger than the mean of the LF's one. For example, with a chosen angle

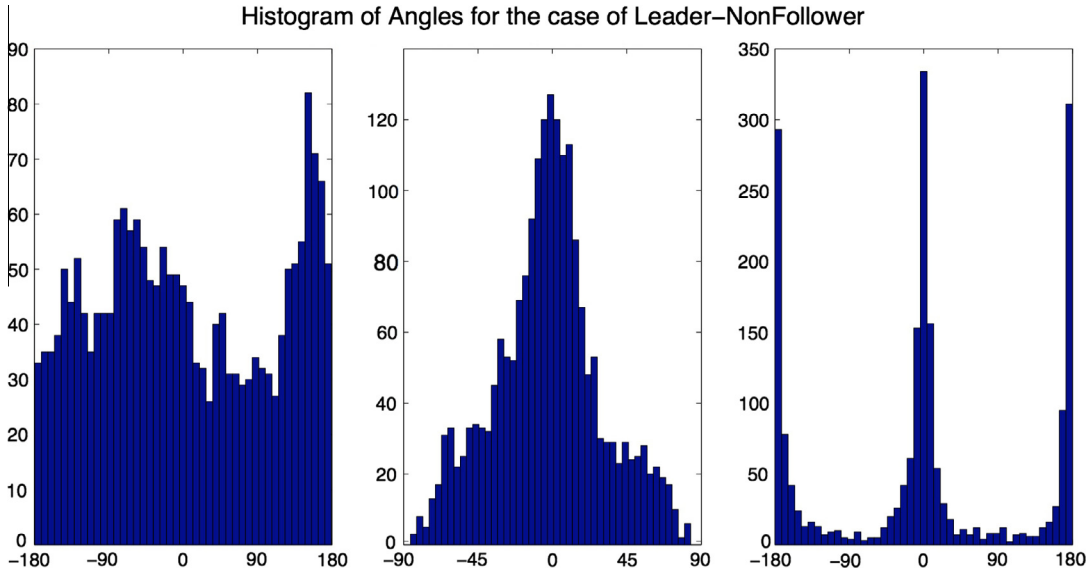

Fig. 6. Yaw, pitch, and roll for the cases of Leader (P_H) and a Non-Follower (P_I).

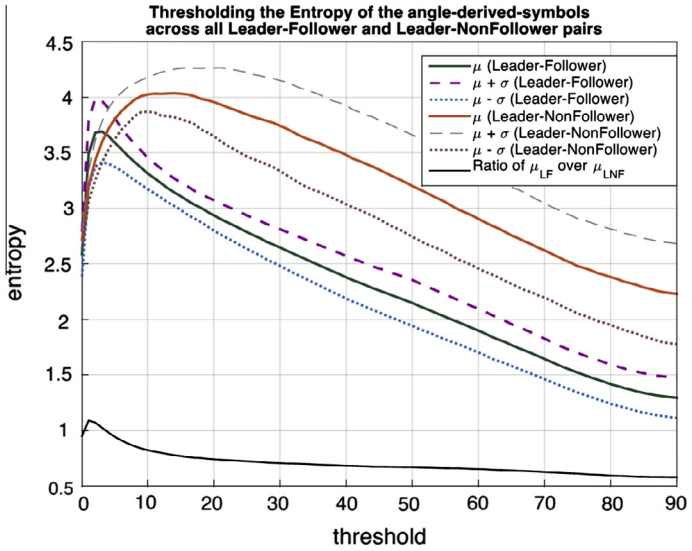

Fig. 7. Entropy means μ and standard-deviations σ, for all LF and LNF pairs in the 4 homing flights, as function of the quantization threshold *Th* for the '0' symbols, and impact on their ratio, assuming that we only use properties Q_7, Q_8, and Q_9 of QTC_{3D}. The slight rise at the beginning is easy to understand: before some meaningful quantization. '0' symbols are almost completely missing, hence the smaller entropy. Once we account for that, however, the entropy quickly drops and, as we discuss in the text, in our dataset the symbol sequences from LNF pairs have always a higher entropy than LF pairs.

threshold $Th = 10^\circ$, the mean entropy for the LF case was 3.36, compared to 4.01 for the LNF case. This can be seen in Fig. 7, which plots the mean entropies as a function of the threshold *Th* for the two cases, as well as their ratio ρ. Furthermore, from the dotted one-standard-deviation bands around the means, also shown in Fig. 7, we clearly have good separation of the distributions of entropy for LF vs. LNF. Therefore, the introduction of the novel symbols Q_7, Q_8, and Q_9 in QTC_{3D}, which accounts for the rotation angles required for matching the Frenet–Serret frames of the moving objects, provides a clear discrimination between qualitatively different pairs of trajectories.

As a further and final elaboration of this result, we performed statistical significance testing, to inquire whether there was support for the hypothesis $\mu_{LF} < \mu_{LNF}$ (i.e. mean entropy of LF smaller than mean entropy of LNF). After removing one clear outlier from the 26 LF pairs through a Grubbs test with probability $P < 0.001$, followed by successful normality testing, we have verified through *t*-testing that our hypothesis holds with $P < 1.5 \cdot 10^{-5}$, for threshold $Th = 10^\circ$. The same hypothesis still holds with significance $P < 0.05$ for a wide range of threshold values, namely any value above $Th > 7^\circ$, even without outlier removal.

Therefore, the entropy ratio criterion generalizes well, and the novel symbols Q_7, Q_8 and Q_9, which were not part of the traditional QTC_{2D}, have certainly contributed to the power and applicability of QTC_{3D} to full three-dimensional interactions.

6. Discussion and future steps

Having introduced QTC_{3D}, and having illustrated its benefits through the bird flight scenario using real-world trajectories, let us now discuss an important point, which is concerned with the need for thresholding. In real world situations, most often apart from time sampling (discrete-time QTC) there is also noise in our trajectory measurements. The problem is that small perturbations in the positions of the MPOs may significantly affect the exported QTC symbols. As an example, consider the cases where two objects would be moving with the same speed. Clearly, even the slightest noise will cause change to the '0' symbol for the speed constraint to become either '+' or '−', and this is unacceptable. Thus, it is very important to define thresholds around zero, but how to set these thresholds? Note that, because of the nature of the equations and the calculations that they imply (Euclidean distances for the distance constraint, cross-products for the Side constraints, etc.) it is not possible to define a meaningful universal threshold for all the QTC constraints.

If we can model the statistical behavior of the noise we are dealing with, we can attempt to fine-tune the thresholds accordingly (analytically or empirically). As a qualitative criterion for optimal tuning, one could try to minimize a reconstruction error, such as the symbol difference between a noise-free zero-threshold QTC sequence and the noisy thresholded version of the sequence. Alternatively, other application-specific criteria can be used for tuning the threshold, including for example variations of discriminability between sequences corresponding to different categories.

Regarding potential application scenarios, an obvious domain would be modeling of insects, airplanes, and unmanned aerial vehicles (UAVs) flight, or even fishes and unmanned underwater vehicles (UUVs). Furthermore, and quite importantly, QTC_{3D} can be utilized not only towards the analysis of trajectories, as is the case in our bird flight example of the previous section, but also towards synthesis: i.e. given a specific QTC sequence, creating behavioral controllers for a robot or UAV/UUV that can perform the correct movements in response to a moving interaction partner, in order to satisfy the prescribed QTC sequence. An example of hand-crafted controller informed by QTC analysis and applied to Human–Robot Spatial Interaction can be found in Bellotto et al. [4]. For the automated solution of the more general problem, which is the generation of prototypical trajectories of two objects satisfying a given QTC sequence, one needs a solution to the so-called "Inverse QTC problem", which was for the first time provided in Iliopoulos et al. [16].

Other interesting application domains are the arts and sports. Group dance movements, for example, contain intricate yet often highly structured patterns of motion; QTC could be used not only towards analysis of human relative trajectories as moving point objects, but also by placing moving point objects at important human body points, and then describing the relative motions within a dancer's body or across dancer's body points [6]. Similar considerations can be made for sports analytics, where QTC_{3D} ould find extensive application, given the importance of the third dimension in this domain.

In terms of future steps, we are currently working not only with the theoretical formalization of thresholding techniques and generalization of the inverse QTC problem, but also with the practical application of QTC in various domains (e.g. robotics, sport, etc.), where a multitude of interesting extensions remain to be explored towards the efficient handling of multiple moving point objects, including groups and centers of symmetry of objects, opening up opportunities for widespread applications of QTC_{3D}.

7. Conclusion

Spatial interactions between natural or artificial agents (humans, animals, or machines) can be found almost everywhere, and carry information of high value to human or electronic observers. However, not all the information contained in a pair of continuous trajectories is important and thus the need arises for adaptive abstractions, such as qualitative descriptions of interaction trajectories.

In this paper we have presented QTC_{3D}, a novel qualitative trajectory calculus that can deal with full three-dimensional interactions, thus moving beyond the limitations of the traditional two-dimensional approach. QTC_{3D} is based on transformations of the Frenet–Serret frames accompanying the trajectories of the moving objects. Apart from the theoretical exposition, including definition and properties, as well as computational aspects, we have also presented in detail a real-world application of QTC_{3D} towards modeling bird flight, using real trajectories, illustrating the benefits of our approach. This opens up a wide range of real-world applications where such representation provides the catalyst for effective analysis and synthesis of complex spatial group behaviors.

Acknowledgements

The authors are very grateful to Dr. Mate Nagy at the Department of Zoology, University of Oxford, for kindly providing the dataset used in our experiments.

References

[1] J. Albath, J.L. Leopold, C.L. Sabharwal, A.M. Maglia, RCC-3D: qualitative spatial reasoning in 3D, in: International Conference on Computer Applications in Industry and Engineering, Las Vegas, Nevada, USA, 2010, pp. 74–79.
[2] J.F. Allen, Maintaining knowledge about temporal intervals, Commun. ACM 26 (11) (1983) 832–843.
[3] N. Bellotto, Robot control based on qualitative representation of human trajectories, in: AAAI Spring Symposium – Designing Intelligent Robots: Reintegrating AI, 2012.
[4] N. Bellotto, M. Hanheide, N. Van de Weghe, Qualitative design and implementation of human–robot spatial interactions, in: Proc. of Int. Conf. on Social Robotics (ICSR), 2013, pp. 331–340.
[5] N. Buch, S. Velastin, J. Orwell, A review of computer vision techniques for the analysis of urban traffic, IEEE Trans. Intell. Transport. Syst. 12 (3) (2011) 920–939.
[6] S.H. Chavoshi, B. De Baets, T. Neutens, H. Ban, O. Ahlqvist, G. De Tré, N. Van de Weghe, Knowledge discovery in choreographic data using relative motion matrices and dynamic time warping, Appl. Geogr. (47) (2014) 111–124.
[7] M. Delafontaine, A.G. Cohn, N. Van de Weghe, Implementing a qualitative calculus to analyse moving point objects, Expert Syst. Appl. 38 (5) (2011) 5187–5196.
[8] M. Delafontaine, N. Van de Weghe, P. Bogaert, P. De Maeyer, Qualitative relations between moving objects in a network changing its topological relations, Inform. Sci. 178 (8) (2008) 1997–2006.
[9] M. Egenhofer, J. Herring, Point-set topological spatial relations, Int. J. Geogr. Inform. Syst. 5 (2) (1991) 161–174.
[10] C. Freksa, Temporal reasoning based on semi-intervals, Artif. Intell. 54 (1992) 199–227.
[11] A. Galton, Qualitative Spatial Change, 2000, 409pp.
[12] L.-J. Guan, M. Duckham, Decentralized reasoning about gradual changes of topological relationships between continuously evolving regions, in: Proceedings of Conference on Spatial Information Theory, 2011, pp. 126–147.
[13] M. Hanheide, A. Peters, N. Bellotto, Analysis of human–robot spatial behaviour applying a qualitative trajectory calculus, in: Proc. of the IEEE Int. Symposium on Robot and Human Interactive Communication (Ro–Man), 2012, pp. 689–694.
[14] F. Heider, M. Simmel, An experimental study of apparent behavior, Am. J. Psychol. 57 (2) (1944) 243–259.
[15] S. Hu, M. Lundgren, A. Niemi, Discrete Frenet frame, inflection point solitons, and curve visualization with applications to folded proteins, Phys. Rev. E 83 (6) (2011).
[16] K. Iliopoulos, N. Bellotto, N. Mavridis, From sequence to trajectory and vice versa: solving the inverse QTC problem and coping with real-world trajectories, in: AAAI Spring Symposium – Qualitative Representations for Robots, 2014.
[17] E. Kreyszig, Differential Geometry, Dover Publications, 1991.
[18] S. LaValle, Planning Algorithms, Cambridge University Press, 2006 (842p).
[19] J.A. Long, T. Nelson, A review of quantitative methods for movement data, Int. J. Geogr. Inform. Sci. 27 (2) (2013) 292–318.
[20] Y. Lu, Discrete Frenet Frame with Application to Structural Biology and Kinematics, PhD Thesis, The Florida State University, 2013.
[21] G. Mather, L. Murdoch, Gender discrimination in biological motion displays based on dynamic cues, in: Proceedings of the Royal Society of London, 1994, pp. 273–279.
[22] M. Nagy, Zs. Akos, D. Biro, T. Vicsek, Hierarchical group dynamics in pigeon flocks, Nature 464 (2010) 890–893.
[23] J. Pacheco, T. Escrig, F. Toledo, Qualitative spatial reasoning on three-dimensional orientation point objects, in: Proc. of the 16th Int. Workshop on Qualitative Reasoning, 2002.
[24] J. Pacheco, T. Escrig, Coarse qualitative model of 3-D orientation, in: M. Polit, T. Talbert, B. Lopez, J. Melendez (Eds.), Artificial Intelligence Research and Development, Book Series: Frontiers in Artificial Intelligence and Applications, vol. 146, 2006, pp. 103–113.
[25] D. Randell, Z. Cui, A.G. Cohn, A spatial logic based on regions and connection, in: Proceedings of Conference on Knowledge Representation and Reasoning, 1992, pp. 165–176.
[26] N. Van de Weghe, Representing and Reasoning about Moving Objects: A Qualitative Approach, PhD Thesis, Ghent University, 2004.
[27] N. Van de Weghe, A.G. Cohn, P. De Maeyer, F. Witlox, Representing moving objects in computer based expert systems: the overtake event example, Expert Syst. Appl. 29 (4) (2005) 977–983.
[28] N. Van de Weghe, A.G. Cohn, B. De Tré, P. De Maeyer, A qualitative trajectory calculus as a basis for representing moving objects in geographical information systems, Control Cybernet. 35 (1) (2006) 97–120.
[29] N. Van de Weghe, P. De Maeyer, Conceptual neighbourhood diagrams for representing moving objects, Lect. Notes Comput. Sci. 3770 (2005) 228–238.
[30] N. Van de Weghe, B. Kuijpers, P. Bogaert, P. De Maeyer, A qualitative trajectory calculus and the composition of its relations, Proc. Geospatial Semantics 3799 (2005) 60–76.
[31] N. Van de Weghe, G. Tré, B. Kuijpers, P. Maeyer, The double-cross and the generalization concept as a basis for representing and comparing shapes of polylines, in: Robert Meersman Zahir Tari, Pilar Herrero (Eds.), OTM Workshops: On the Move to Meaningful Internet Systems 2005, Springer, Berlin Heidelberg, 2005, pp. 1087–1096.
[32] B. Zhan, D. Monekosso, P. Remagnino, S. Velastin, L.-Q. Xu, Crowd analysis: a survey, Mach. Vision Appl. 19 (5–6) (2008) 345–357.